Available online at www.sciencedirect.com
SCIENCE DIRECT®
Nuclear Instruments and Methods in Physics Research A 509 (2003) 283–289
NUCLEAR INSTRUMENTS & METHODS IN PHYSICS RESEARCH Section A
www.elsevier.com/locate/nima

Semiconductor pixel detectors for digital mammography

M. Novelli[a,*], S.R. Amendolia[b], M.G. Bisogni[a], M. Boscardin[c], G.F. Dalla Betta[c,d], P. Delogu[a], M.E. Fantacci[a], M. Quattrocchi[e], V. Rosso[a], A. Stefanini[a], L. Venturelli[f], S. Zucca[a]

[a] *Dipartimento di Fisica, Università di Pisa and Sezione INFN, Via Buonarroti 2, Pisa 56100, Italy*
[b] *Istituto di Matematica e Fisica, Università di Sassari and Sezione INFN, Pisa, Italy*
[c] *ITC-irst, Divisione Microsistemi, Trento, Italy*
[d] *Dipartimento di Informatica e Telecomunicazioni, Università di Trento, Italy*
[e] *Dipartimento di Fisica, Università di Napoli and Sezione INFN, Pisa, Italy*
[f] *Alenia Marconi Systems S.p.A., Roma, Italy*

Abstract

We present some results obtained with silicon and gallium arsenide pixel detectors to be applied in the field of digital mammography.

Even though GaAs is suitable for medical imaging applications thanks to its atomic number, which allows a very good detection efficiency, it often contains an high concentrations of traps which decrease the charge collection efficiency (CCE). So we have analysed both electrical and spectroscopic performance of different SI GaAs diodes as a function of concentrations of dopants in the substrate, in order to find a material by which we can obtain a CCE allowing the detection of all the photons that interact in the detector. Nevertheless to be able to detect low contrast details, efficiency and CCE are not the only parameters to be optimized; also the stability of the detection system is fundamental. In the past we have worked with Si pixel detectors; even if its atomic number does not allow a good detection efficiency at standard thickness, it has a very high stability. So keeping in mind the need to increase the Silicon detection efficiency we performed simulations to study the behaviour of the electrical potential in order to find a geometry to avoid the risk of electrical breakdown.

PACS: 87.59

Keywords: Medical imaging; GaAs; Si pixel detectors

1. Introduction

Our group is working at the development of a prototype for digital mammography based on semiconductor detection systems (assemblies). Each assembly is composed by a semiconductor pixel detector and a single photon counting chip (PCC, developed within the framework of the MEDIPIX collaboration [1–3]). The chip contains 64×64 square cells, 170 μm in side, connected to each pixel of the detector by bump bonding. The possibility to detect tumoral masses, i.e.

*Corresponding author. Tel.: +39-050-2214-397; fax: +39-050-2214-333.
E-mail address: marzia.novelli@pi.infn.it (M. Novelli).

0168-9002/03/$ - see front matter
doi:10.1016/S0168-9002(03)01639-5

pathological objects which at their early stage of development show relatively big dimensions (at least of the order of many mm in diameter) but very low contrast (of the order of 1%), is one of the characteristics of the our under development prototype as regards to the traditional film screen systems. We have showed that working with assemblies based on 200 μm thick GaAs detector [4] and with 300 μm thick Si detector [5], we were able to detect low contrast details using the same exposition conditions regardless to the different detection efficiency of the semiconductors (for γ of $\sim$22 keV, 200 μm thick GaAs has a detection efficiency near to 100%, while 300 μm thick Si has a detection efficiency of $\sim$20%). We can explain these results in term of the superior stability and homogeneity of the Si-based system; these qualities are necessary because the procedure to obtain the final image require to equalize, by weighting, the acquired image with an image of a flat field.

In this work we describe the electrical and spectroscopic characterization of SI GaAs detectors, produced starting from crystals grown with different techniques, supplied by different manufacturers and with different concentrations of the dopants in the bulk, namely carbon and chromium. We present also the studies of Si detectors. In particular we have simulated the behaviour of the electric potential inside the detector in order to find a geometry to optimize the performances of our detector and to avoid the risk of breakdown that will be more likely as one will increase the thickness. A first batch of Si detectors have been designed and fabricated at ITC-IRST, Trento (Italy), with 300 and 525 μm thickness. We present the results of the performances of some single diodes of this batch.

2. Si–GaAs detectors with dopants

The SI GaAs detectors under investigation are single diode structures with a thickness of 200 μm. They were processed by AMS (Alenia Marconi Systems) in Roma (Italy) from 3 in. wafers supplied by different factories. The crystals are $\langle 1\,0\,0 \rangle$ oriented, Liquid Encapsulate Chocralsky (LEC) and Vertical Gradient Frozen (VGF) grown and doped with carbon and chromium.

On one side the Schottky contact, a Ti/Pt/Au multilayer, was evaporated to obtain circular pads with a diameter of 2 mm while on the other side a common not-alloyed Ohmic contact was realized [6].

In Table 1 the characteristics of the different GaAs detectors are listed. The first four detectors have an uncontrolled, but lower than $10^{15}\,cm^{-3}$, carbon concentration and in the fourth also a known chromium concentration is present. The last three detectors have three different controlled carbon concentrations.

It is important to keep the operating reverse voltage far away from the breakdown in order to have a uniform and stable response, that will permit a good image quality and charge collection efficiency (CCE). To study the performance of our detectors in terms of leakage current and CCE when irradiated, we have tested them up to 500 V. We qualify a detector as a good one when the leakage current is lower than 50 nA/mm^2 and CCE is greater than 75%.

Table 1
Summary of the characteristics of the different GaAs detectors

Manufacturers	Material	Type of growing	Doping
Freiberger Compound Materials	FRE	LEC	$[C] < 10^{15}\,cm^{-3}$
MCP Wafer Technology Limited	MCP	LEC	$[C] < 10^{15}\,cm^{-3}$
American Xtal Technology	AMXC 2065	VGF	$[C] < 10^{15}\,cm^{-3}$
Sumitomo	SMT 1 CR	LEC	$[C] < 10^{15}\,cm^{-3}$ $[Cr] = 1 \times 10^{17}\,cm^{-3}$
Nippon Mining	ACR 068	LEC	$[C] = 1.3 \times 10^{15}\,cm^{-3}$
Nippon Mining	ACR 013	LEC	$[C] = 5 \times 10^{15}\,cm^{-3}$
Nippon Mining	ACR 079	LEC	$[C] = 1 \times 10^{16}\,cm^{-3}$

For each diode we have made both an electrical and a spectroscopic characterization.

2.1. Electrical characterization

The measurements of the electrical properties of SI GaAs detectors have been performed using a picoammeter/voltage source (KEITHLEY mod.487) and applying a reverse voltage on the Schottky contact up to a value of 500 V.

In Figs. 1 and 2 the current density is represented as a function of the reverse voltage for all the seven different types of detector materials. Fig. 1 refers to the three diodes with a defined carbon concentration while Fig. 2 to all the other diodes.

The behaviour of the current densities reproduce that of a reverse biased diode and, in the case of Fig. 1, the differences between the current density curves are in agreement with the differences in the doping concentrations. In fact we can observe that the current density decreases as the carbon concentration becomes higher, because this increases the material resistivity. Detectors do not suffer breakdown problems up to a reverse voltage of 500 V. As for the diodes of Fig. 2, the relatively high values of the leakage current density can suggest that their carbon concentration is much lower than $10^{15}\,cm^{-3}$, except for the diode doped with chromium, whose leakage current curve at low bias voltages is comparable to that of the detector of Fig. 1 having the lowest carbon concentration. Nevertheless, this diode exhibits electrical breakdown at about 250 V.

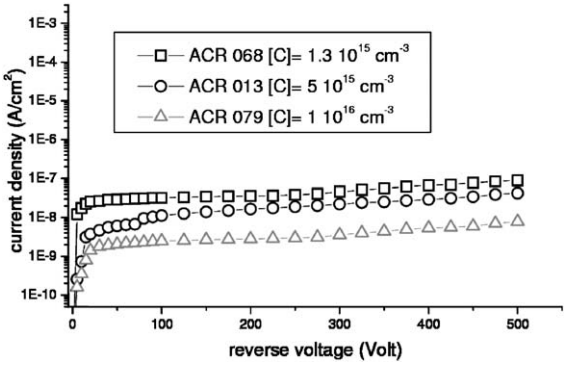

Fig. 1. Current density as a function of the reverse voltage for SI GaAs single diodes with a well-controlled carbon concentrations.

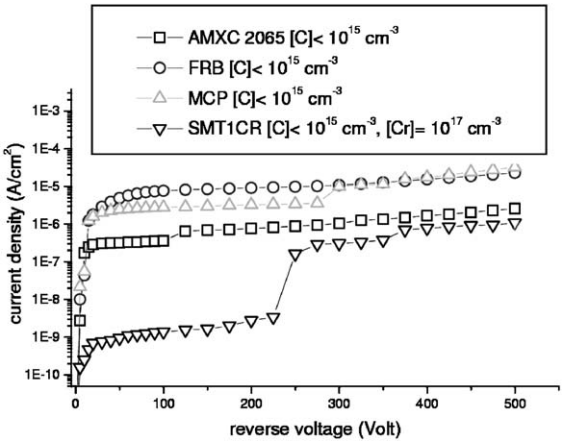

Fig. 2. Current density as a function of the reverse voltage for SI GaAs single diodes without a well-controlled carbon concentrations.

2.2. Spectroscopic characterization

To evaluate the spectroscopic properties of GaAs detectors we have used a charge-sensitive preamplifier ORTEC142A, a shaper amplifier ORTEC673 with a shaping time of 1.5 μs and a multichannel analyser (NUCLEUS-PCA II).

The detectors have been irradiated with ^{241}Am source (59.54 keV photons) from the side of the Schottky contact and the spectra have been acquired increasing the bias voltage, starting from 50 V with a step of 50 V.

The responses of the detectors not having a well-defined carbon concentration and of the detector doped with chromium were not good. Almost all the detectors, when irradiated, have shown a signal that was not well separated from the noise; only the ACR 068 material has shown good spectroscopic properties.

For this diode we have calculated the CCE as a function of the bias voltage. We have performed a Gaussian fit and we have used the mean value to evaluate the CCE and the σ to evaluate the noise. As can be seen in Fig. 3, the CCE increases as the reverse bias is increased, until a plateau region is

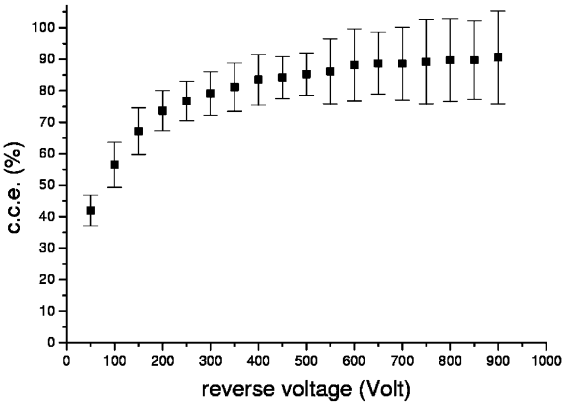

Fig. 3. CCE as a function of the reverse voltage for a SI GaAs single diode made from ACR 068 material.

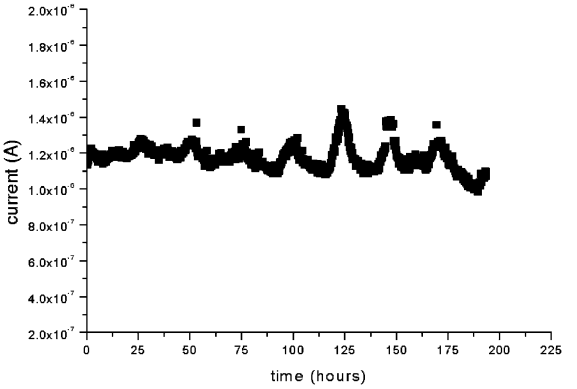

Fig. 4. Leakage current as a function of the time for a GaAs matrix of 64×64 square pixels.

reached where a very high value of CCE, in the order of 90%, is obtained.

To be sure of the obtained results we have tested 10 single diodes of the same material. We have found that the behaviour of the current density and of the CCE is the same for all the detectors within the experimental errors shown in Fig. 3.

As a result, for this set of detectors, the optimal carbon concentration from the spectroscopic viewpoint is $1.3 \times 10^{15}\,\mathrm{cm}^{-3}$. So we have decided to use a Sumitomo material having a concentration in the range $(1 \times 10^{15}$–$1.3 \times 10^{15})\,\mathrm{cm}^{-3}$ nevertheless they are easier to find as regards the other manufacturers. The performance of these detectors in term of CCE are comparable to the one of the ACR 068 material [7,8] and are in agreement with our specific requests in term of leakage current and CCE.

Thus AMS realized matrices of 64×64 square pixels, 170 μm in side, from wafers supplied by Sumitomo. To test the stability of the detectors when biased, some pixel detectors were connected to a golden alumina via bump bonding by AMS, in this way we were sure that all the detector volume was completely depleted.

We have measured the electrical characteristics of these GaAs matrices applying a reverse voltage on the back side of the detector up to a value of 500 V (using a picoammeter/voltage source KEITHLEY mod.487). The leakage current values were very low. At a reverse bias voltage of 350 V the current, for all the detectors, was lower than 2 μA. The breakdown voltage was of the order of 420 V for 2 of the measured detectors, for another one was 460 V and one did not exhibit breakdown. So a detector has been polarized at 350 V and maintained at this voltage for at least 200 h, reading the current every 15 min. In Fig. 4 the behaviour of the current as a function of the time is shown. The current varies around a mean value of 1.2 μA with a maximum fluctuations of 17%. All the peaks in the current are in correspondence of the increment of the temperature in the laboratory during the days.

3. Simulation of Si detectors

3.1. Numerical device simulation

As regards Silicon detectors we have started to work with ITC-IRST in Trento (Italy). In particular we are interested, as previously told, to produce Si detectors thicker than 300 μm to increase the detection efficiency. As starting point we have decided to simulate, produce and test the 300 and 525 μm thick pixel detectors. We have used numerical device simulations to study the behaviour of the electric potential inside the detectors. Simulations were performed by means of the 2-D device-analysis program DESSIS, included in the T-CAD software package by ISE AG [9]. DESSIS solves Poisson's and carrier continuity equations, with electron and hole

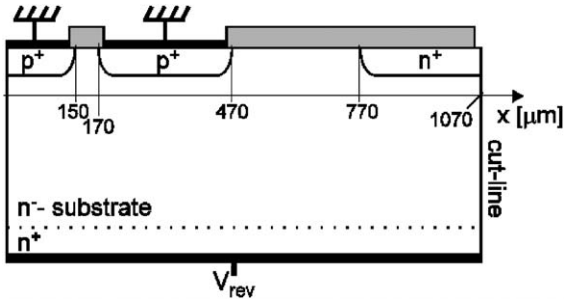

Fig. 5. Schematic cross-section (not to scale) of the simulated Si detector without multiple rings.

current densities given by the drift-diffusion model. All main physical effects of interest in device modelling are supported. The values of the main parameters, chosen as representative of the fabrication technology [10] and adopted in the simulations, are: substrate–donor concentration $N_{sub} = 5 \times 10^{11}\,cm^{-3}$, oxide thickness $t_{ox} = 1\,\mu m$, fixed charge density at the Si–SiO_2 interface $N_{ox} = 4 \times 10^{11}\,cm^{-2}$, bulk-generation lifetime $\tau_g = 100\,ms$, surface-generation velocity $s_0 = 25\,cm/s$.

At first we have simulated the structure sketched in Fig. 5. On the front side there is a 150 μm wide p^+-implant, representing a pixel, followed at a distance of 20 μm by a second p^+-implanted guard ring, 300 μm wide. At the device edge, at 300 μm from the guard ring, there is a 300 μm wide n^+-implant including the scribe line. On the backside there is a uniform n^+-implant providing a large ohmic contact. The two p^+-implants are grounded, whereas a positive bias voltage, V_{rev}, is applied to the backside n^+-implant. The silicon substrate is 300 μm thick.

We have simulated the 2-D electric potential distribution across the Silicon bulk at a reverse bias voltage of 100 V. In this condition the substrate is fully depleted, and the Space Charge Region (SCR) extends also laterally. However, at the surface the electrons in the accumulation layer underneath the passivation oxide counteract this lateral extension and the applied voltage drops rapidly, so that a high electric field appears close to the Si–SiO_2 interface.

Starting from the structure of Fig. 5 we inserted on the frontside a multiple guard ring termination structure in between the main guard ring and the

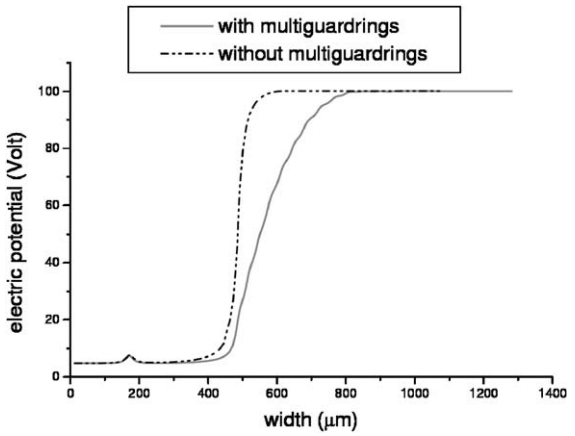

Fig. 6. Comparison of the simulated electric potential across a section taken at the Si–SiO_2 interface of Si detectors with and without multiple guard rings.

n^+-implant [11,12]. This structure consists of 12 p^+-implanted floating rings ($G_1 \ldots G_{12}$), all of them having a width of 15 μm: the distance between each pair of adjacent rings increases from 15 to 30 μm every three rings moving from the centre to the device edge. Floating rings are all provided with a metal overhang extending inward and outward by 5 μm with respect to the p^+-implant. The total traversal dimension was of 1270 μm.

The simulated 2-D electric potential distribution for the structure of Fig. 6 at a reverse bias voltage of 100 V has shown that the SCR spreads laterally much further than in the case of the single guard ring, as a result of punch-through conduction between the rings. At 100 V bias voltage, 8 rings out of 12 are reached by the SCR, so that the surface potential drops across a longer distance with respect to the geometry described in Fig. 5. The design of the guard rings is well balanced to limit the field strength in the depleted region and to prevent the SCR from reaching the device edge, where surface generation occurs and excess leakage can be drawn to the main junction via punch-through conduction across the guard rings.

The behaviour of the electric potential and of the electric field across the width of the detectors at the Si–SiO_2 interface is compared for the two types of structures in Figs. 6 and 7. A more gentle drop

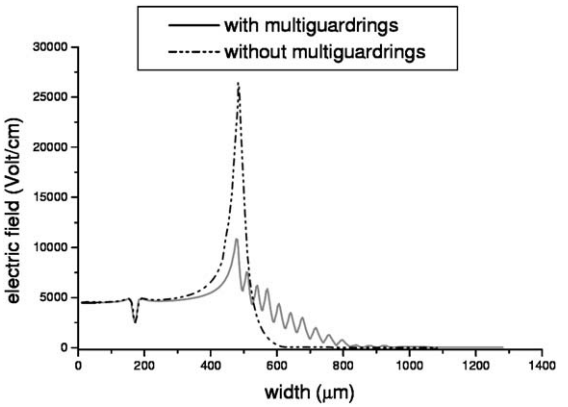

Fig. 7. Comparison of the simulated electric field across a section taken at the Si–SiO_2 interface of Si detectors with and without multiple guard rings.

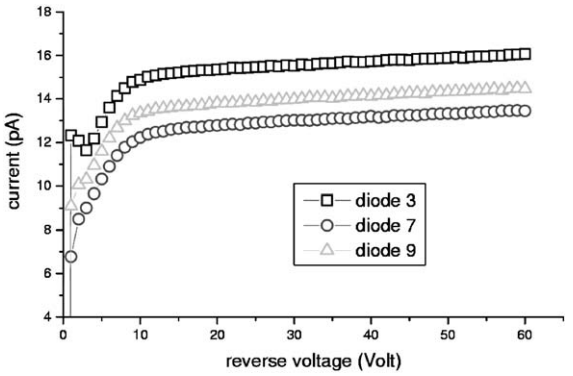

Fig. 8. Leakage current as a function of the reverse voltage for three Si test diodes with guard ring.

of the electric potential from the cutting edge towards the active region is evident for the structure with multiple guard rings, and, as a result, the peak electric field is considerably reduced, thus lowering the risk of breakdown.

The termination structure with multiple guard rings has been implemented in the layout of a first batch of p^+/n silicon detectors recently fabricated at ITC-IRST, Trento (Italy). The production has involved the processing of 12 wafers, 4 in. in diameter and 300 and 525 μm in thickness.

3.2. Electrical characterization of wafers

To check the properties of the wafers produced at ITC we have tested some single diodes. Diodes are circular, 2 mm in diameter, and are equipped with a first guard ring of 300 μm, placed at a distance of 8 μm from the diode, and a second guard ring of 150 μm placed at a distance of 30 μm from the first guard ring.

In Fig. 8 the current drawn by the central diode is plotted as a function of the reverse voltage for three samples belonging to one of the 300 μm thick wafers.

All the measures are performed in the same environmental conditions (temperature = 21.5°C, humidity = 65%). The leakage current values are very low, in the range 12–15 pA at full depletion, corresponding to a current density lower than 0.5 nA/cm^2, with good on-wafer uniformity. These values are in agreement with the simulated results, which give a leakage current of 16 pA. The peculiar behaviour of the current of diode 3 at low voltage may be ascribed to the diffusion current that can reach the diode since the substrate is not completely depleted [13]. While increasing the reverse voltage the diode is fully depleted (at about 10 V), and the guard ring can behave as a perfect shield for the diode. Similar results have been obtained from diodes belonging to the 525 μm thick wafers, that of course feature a much higher depletion voltage (about 100 V) as a result of the much higher substrate thickness.

Further measurements have been performed on other test diodes equipped with the same 12 floating rings implemented in the pixel detector layout. Diodes are square shaped ($1.08 \times 1.08\ mm^2$) and are surrounded by a main guard ring, 300 μm wide, that, in turn, is surrounded by the 12 floating rings. The very high voltage handling capability of the termination structure is demonstrated in Fig. 9, which shows the diode and main guard ring currents as a function of reverse voltage up to 1100 V (limit set by the available instrumentation). In fact, most of the measured diodes exhibit breakdown voltage exceeding 1100 V, and only less than 10% of the diodes suffer breakdown at a reverse voltage lower than 500 V, evidence of the good quality of the design and of the fabrication technology.

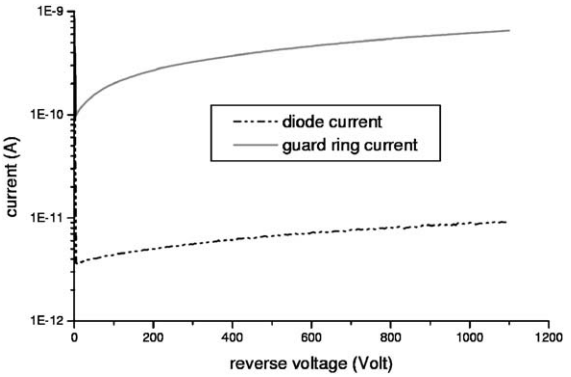

Fig. 9. Diode and main guard ring currents as a function of the reverse voltage for a test diode featuring the same 12 ring termination structure adopted for the Si pixel detector.

4. Conclusions

In this work we have compared the results of the characterization of GaAs detectors with different types and concentrations of the dopants. We have obtained that, in order to have the best spectroscopic performances the type of dopants is carbon with a concentration in the range $(1.0 \times 10^{15}$–$1.3 \times 10^{15})\,\mathrm{cm}^{-3}$.

Besides we have defined the geometry for Silicon detectors making use of numerical device simulations. We have designed and produced different Si detectors and we started testing some diodes: the measurements confirmed the simulated results.

At the moment GaAs detectors with the chosen carbon concentration are ready and they will be bump bonded to the dedicated electronic chip by AMS (Italy), while Si detectors are in phase of bump bonding by VTT (Finland) and also by AMS (Italy).

As soon as possible we will start to check the imaging performances of these devices.

Acknowledgements

We would like to thank A. Cetronio and C. Lanzieri of AMS (Alenia Marconi Systems) in Roma (Italy) for making available SI–GaAs detectors with different dopants and for the helpful discussions and N. Zorzi and P.Gregori of ITC-IRST in Trento (Italy) for the help in the testing measures.

References

[1] http://medipix.web.cern.ch/MEDIPIX.
[2] M.G. Bisogni, et al., Proc. SPIE 3445 (1998) 298.
[3] M. Campbell, et al., IEEE Trans. Nucl. Sci. NS-45 (3) (1998) 751.
[4] S.R. Amendolia, et al., IEEE Trans. Nucl. Sci. NS-47 (4) (2000) 1478.
[5] S.R. Amendolia, et al., Imaging and Spectroscopic Performances For a Si Based Detection System, in: Proceedings of the IEEE Nuclear Science Symposium on Medical Imaging Conference, 0-7803-6503-8/01 4–123/126.
[6] M. Alietti, et al., Nucl. Instr. and Meth. A 362 (1995) 344.
[7] S.R. Amendolia, et al., Nucl. Instr. and Meth. A 434 (1999) 14.
[8] S.R. Amendolia, et al., Study of GaAs detectors characteristics for medical imaging, in: Proceedings of International Workshop on Room-Temperature Semiconductor X- and Gamma-Ray Detectors, San Diego (CA) November 5, 2001; 0-7803-7324-3/02.
[9] DESSIS6.0 Reference Manual, ISE Integrated Systems Engineering AG, Zürich (Switzerland), 1999.
[10] G.F. Dalla Betta, et al., Nucl. Instr. and Meth. A 460 (2001) 303.
[11] M. Da Rold, et al., IEEE Trans. Nucl. Sci. NS-46 (4) (1999) 1215.
[12] T. Rohe, Nucl. Instr. and Meth. A 460 (1) (2001) 55.
[13] G. Simi, et al., Nucl. Instr. and Meth. A 485 (2002) 193.